NAVAL POSTGRADUATE SCHOOL
Monterey, California

THESIS

SENSITIVITY OF THE CALIFORNIA COASTAL JET TO SYNOPTIC SCALE FLOW

by

R. Scott Stevens

September, 1997

Thesis Advisor: Wendell Nuss

Approved for public release; distribution is unlimited.

REPORT DOCUMENTATION PAGE			Form Approved OMB No. 0704-0188

1. AGENCY USE ONLY *(Leave blank)*	2. REPORT DATE September, 1997	3. REPORT TYPE AND DATES COVERED Master's Thesis

4. TITLE AND SUBTITLE SENSITIVITY OF THE CALIFORNIA COASTAL JET TO SYNOPTIC SCALE FLOW	5. FUNDING NUMBERS
6. AUTHOR(S) R. Scott Stevens	

7. PERFORMING ORGANIZATION NAME(S) AND ADDRESS(ES) Naval Postgraduate School Monterey CA 93943-5000	8. PERFORMING ORGANIZATION REPORT NUMBER

9. SPONSORING/MONITORING AGENCY NAME(S) AND ADDRESS(ES)	10. SPONSORING/MONITORING AGENCY REPORT NUMBER

11. SUPPLEMENTARY NOTES The views expressed in this thesis are those of the author and do not reflect the official policy or position of the Department of Defense or the U.S. Government.

12a. DISTRIBUTION/AVAILABILITY STATEMENT Approved for public release; distribution is unlimited.	12b. DISTRIBUTION CODE

13. ABSTRACT *(maximum 200 words)*

The California Coastal Jet can have a significant impact on many operations. This study examines the sensitivity of the California Coastal Jet to the synoptic-scale flow by examining the surface reflection of the jet at a particular buoy (buoy 46028) off the Central California coast. Statistical analysis and subjective examination of surface charts were performed to help determine the relationship between the synoptic flow regime and the observed surface winds. The main results of the study are as follows:

- The magnitude of the California Coastal Jet is sensitive to the geostrophic wind direction.
- The surface reflection of the California Coastal Jet at buoy 46028 does not exhibit diurnal variation. The day to day variability in the observed winds is much larger than the diurnal variation at buoy 46028.
- Higher wind speed events at buoy 46028 correspond to periods when the synoptic analyses are not performing adequately (meso-scale effects such as flow blocking and supercritical flow are missed in the model). Lower wind speed events correspond to periods when the synoptic-scale analyses are performing adequately.

Recommendations for future study are made.

14. SUBJECT TERMS CALIFORNIA COASTAL JET, FLOW BLOCKING, SUPERCRITICAL FLOW			15. NUMBER OF PAGES 58
			16. PRICE CODE

17. SECURITY CLASSIFICATION OF REPORT Unclassified	18. SECURITY CLASSIFICATION OF THIS PAGE Unclassified	19. SECURITY CLASSIFICATION OF ABSTRACT Unclassified	20. LIMITATION OF ABSTRACT UL

SENSITIVITY OF THE CALIFORNIA COASTAL JET TO SYNOPTIC SCALE FLOW

R. Scott Stevens
Lieutenant, United States Navy
B.S., University of Washington, 1992

Submitted in partial fulfillment
of the requirements for the degree of

MASTER OF SCIENCE IN METEOROLOGY AND PHYSICAL OCEANOGRAPHY

from the
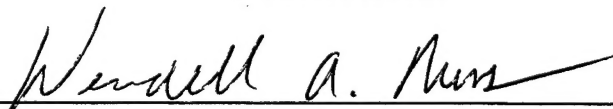
NAVAL POSTGRADUATE SCHOOL
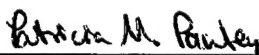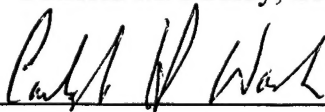**September 1997**

Author: _____
R. Scott Stevens

Approved by: _____
Wendell A. Nuss, Thesis Advisor

_____
Patricia M. Pauley, Second Reader

_____
Carlyle H. Wash, Chairman, Department of Meteorology

iii

iv

ABSTRACT

The California Coastal Jet can have a significant impact on many operations. This study examines the sensitivity of the California Coastal Jet to the synoptic-scale flow by examining the surface reflection of the jet at a particular buoy (buoy 46028) off the Central California coast. Statistical analysis and subjective examination of surface charts were performed to help determine the relationship between the synoptic flow regime and the observed surface winds. The main results of the study are as follows:

▶ The magnitude of the California Coastal Jet is sensitive to the geostrophic wind direction.

▶ The surface reflection of the California Coastal Jet at buoy 46028 does not exhibit diurnal variation. The day to day variability in the observed winds is much larger than the diurnal variation at buoy 46028.

▶ Higher wind speed events at buoy 46028 correspond to periods when the synoptic analyses are not performing adequately (meso-scale effects such as flow blocking and supercritical flow are missed in the model). Lower wind speed events correspond to periods when the synoptic-scale analyses are performing adequately.

Recommendations for future study are made.

TABLE OF CONTENTS

I. INTRODUCTION

Those who have spent a fair amount of time on the California coastal waters can attest that the magnitude of the coastal winds are often much greater than forecast or even analyzed. The primary reason for these strong coastal winds is the existence of the California Coastal Jet, which is a semi-permanent low-level feature that persists through the late spring and summer months off the northern and central California coast. The presence of this jet has a significant impact on mariners, commercial fishermen, firefighters, environmentalists, aviators, recreationalists, urban developers, as well as the Department of Defense. Sparse data and the inability of numerical models to properly incorporate topographic and mesoscale effects contribute to the challenge of analyzing and forecasting the magnitude of the California Coastal Jet. The ability to forecast or even nowcast the onset of enhanced winds would increase safety and productivity for those listed above to save time and money.

The California Coastal Jet is primarily driven by the pressure gradient between the synoptic-scale North Pacific High centered near 40° N 140° W and the thermally generated low pressure which exists over the western United States. The pressure distribution between these primary features gives

1

rise to the climatological northwesterly surface winds along the California coast during the summer. Associated with the surface high pressure is large-scale subsidence, which gives rise to a persistent low-level inversion over the cool waters of the eastern Pacific ocean. These features combine to produce a low-level coastal jet through much of the warm season; however, the considerable day-to-day variation in the surface winds along the coast indicates that the jet may be sensitive to a variety of factors.

The structure and basic dynamics of the coastal jet have previously been attributed to the strong coastal baroclinity caused by the differential diurnal heating of the land and the cold upwelled waters off the California coast. As described by Burk and Thompson (1995), the coastal baroclinity produces a thermal wind turning of the low-level winds, which results in the strongest geostrophic northwesterly flow at the surface. Frictional effects force the wind maxima to occur above the surface near the top of the boundary layer. Burk and Thompson (1995) describe the diurnal movement in position of the jet and contend that the jet maximum lags the maximum baroclinity by 6 hours, with the maximum baroclinity occurring at 1600 PDT and the jet maximum occurring at 2200 PDT. They attribute the time lag between the maximum baroclinity and the jet maximum to the presence of inertial motions.

The presence of the low-level inversion has several impacts on the coastal jet also. First, given the height of the inversion, which is typically below the top of the coastal mountains, the inversion is likely to produce flow blocking of the cross-coast wind by the coastal mountains. Flow blocking results when air impinging upon a mountain barrier has insufficient kinetic energy to go over the mountain barrier in the presence of strong stability. The result is to turn the flow into the along-barrier direction and to accelerate the air down the along-barrier pressure gradient. The role that flow blocking plays in the formation and dynamics of the coastal jet has not been explored in previous studies. The tendency of the coastal winds to remain primarily parallel to the coast during summer is most likely the result of flow blocking. This also suggests that synoptic scale flow changes that alter the cross-coast wind component may impact the coastal jet through increases or decreases in the relative effects of blocking.

The low-level inversion in combination with the winds may also give rise to supercritical flow effects. Winant et al (1988) have shown these supercritical flow effects along one portion of the coastline but the general applicability to other regions along the coast under a variety of flow conditions is not well known. As described by Winant et al

3

(1988), supercritical flow is believed to occur along the downwind side of points and capes along the California coast when the surface winds reach some critical magnitude and the Froude number is greater than one, such that a hydraulic jump occurs ahead of the region of maximum winds as the flow adjusts to the new boundary.

This study examines the hypothesis that the California Coastal Jet is sensitive to the synoptic-scale wind direction and that enhanced winds near Point Sur are due to flow blocking and supercritical flow. The objectives of the study are to illustrate how and to what extent the California Coastal Jet is sensitive to the synoptic scale flow, to illustrate how and to what extent the California Coastal Jet exhibits diurnal variation, and to highlight and exemplify the relationship between the coastal wind and the ETA model analysis of the thermal, pressure, and resultant wind fields in the California coastal region.

II. DATA

The data used for the study were collected during the three-month period from June through August 1994. The data consist of routine surface observations from buoys along the California coast, special rawinsonde observations taken at the Naval Postgraduate School in Monterey, California, and at Fort Hunter Liggett in Jolon, California, plus rawinsonde observations taken from R/V SPROUL off the California coast during one period in August. In addition, vertical wind profiler data were collected from 915 MHZ vertical wind profilers at Fort Ord in Marina, California, and at Point Sur along the coast to the south of Monterey.

In addition to these observations, early ETA model analyses were used to produce the synoptic charts for this study. The early ETA model is an 80 km resolution model with 38 layers that utilizes an early data cutoff in its data assimilation cycle. The analysis cutoff occurs one hour and 15 minutes after the analysis time, and the analysis uses multi-variate optimum interpolation (MVOI). The optimum interpolation weights are calculated at each grid point by using the nearest 30 observation locations. The analysis is multi-variate, such that height increments affect the wind analysis and wind increments effect the height analysis. The

30 weighted observation increments are summed to form an analysis increment at each grid point, which is combined with the first-guess values to form the full-field analysis (Black et al, 1993).

The upper-air profiling system utilized for the study was the Vaisala-Digicora receiver-processor and RS80-series rawinsondes. The measurements were made using free-ascent balloon rawinsondes. The observed surface wind is used as the surface wind in the profiles. The wind samples above the surface are calculated by utilizing the Grubbs algorithm. The wind samples are evaluated every 10 seconds. A four-minute value is calculated consisting of 24 - "10 second" values. The algorithm smooths the wind data and heavily weights the wind values around the mean 2-minute layer. This technique approximates a radar 2-minute wind value. As additional 10-second wind values are accumulated, the 4-minute value is recalculated, giving a running calculation based on the latest data. The wind values for the standard levels are taken directly from the value nearest to that level if the time difference is less than 10 seconds. Otherwise, an interpolation is carried out unless the time interval exceeds four minutes. Hence, the vertical resolution of the data is approximately 500 meters.

The vertical wind profiler data from the Marina location

and the Point Sur profiler was collected in low mode. The low mode provided winds at 60 meter vertical resolution and the associated radio acoustic sounding system (RASS) provided virtual temperature observations with comparable resolution. The useable data from the profilers ranged from the surface to approximately 1500 meters. All the data used in this study are archived and available from the Department of Meteorology, Naval Postgraduate School Monterey, California.

III. DATA ANALYSIS

The rawinsonde and vertical wind profiler data were examined to determine the height and the strength of the inversion and to examine its relationship to the coastal wind. The rawinsonde plots were also used to determine a general synoptic-scale wind direction, using a representative height of 700 mb. The 700 mb level was chosen because it is above the Marine atmospheric Boundary Layer (MABL) and it is significantly higher than the coastal topography. Additionally, the 700 mb flow direction from the Monterey sounding was compared to the 700 mb flow direction from the in land location to ensure that local topographic and mesoscale effects did not impact on the flow characterization.

Synoptic-scale surface analyses were constructed to characterize the variability of the observed winds at the coastal buoy locations relative to the synoptic-scale pressure analysis. The ETA model mean sea-level pressure and isotherm analyses were plotted with ship and buoy observations to construct synoptic scale surface charts for the Eastern Pacific Ocean. These surface analyses were plotted for 0000 UTC and 1200 UTC daily for the three months of the study using the analysis and the display software VISUAL (Nuss and Drake, 1993).

9

To assess the relative strength of the observed coastal winds compared to the synoptic-scale model-analyzed winds, difference plots were constructed for each analysis time using VISUAL (Nuss and Drake, 1993). The difference plots were constructed by plotting the observed wind minus the model analyzed wind as barbs at every observation point. To show the character of the synoptic-scale winds, the model-analyzed wind barbs were also included on each plot. Fig. 1 shows an example of one of these difference plots. The figure clearly shows large wind differences at the coastal buoy locations and smaller differences at offshore ships and buoys. These differences arise from the fact that the ETA model analysis is tuned to analyze the large synoptic scale which ignores mesoscale coastal effects that influence the observed coastal winds. The MVOI analysis produces a wind analysis that is consistent with the sea-level pressure analysis as is evident in Fig. 1.

To characterize the ageostrophic nature of the observed coastal winds, similar difference plots were generated using the observed wind from the ships and buoys and the synoptic-scale geostrophic wind from the model analyses. Vector plots illustrating the geostrophic wind direction and relative magnitude with the wind differences (observations minus the model analyzed geostrophic) plotted at the observation sites

10

using VISUAL (Nuss and Drake, 1993). Fig. 2 shows an example of such a plot. Note that the coastal wind difference in this case arises from both scale differences and factors such as friction that can produce ageostrophic wind components. The figure shows that the coastal winds tend to be highly ageostrophic flowing nearly straight down the pressure gradient. These geostrophic flow charts were used to determine the direction of the geostrophic wind relative to the coast near buoy 46028 (buoy 28), which was selected for more detailed statistical analysis. Buoy 28 is located offshore south of Pt. Sur.

To quantitatively evaluate the character of the coastal winds and their relationship to the synoptic-scale structure, statistical analysis was done for a single coastal buoy. Buoy 28 was chosen because of its proximity to other data sources and because the coastline near buoy 28 is fairly representative of much of the Northern and Central California coast. The observed u and v wind components, the model analyzed u and v wind components, the difference u and v wind components, and the model analyzed geostrophic u and v wind components were tabulated. These data tables were then used to calculate the wind speed and direction of the observed wind, model analyzed wind, the difference between the observed and model analyzed wind, model analyzed geostrophic wind, and

11

the difference between the observed wind and the model analyzed geostrophic wind. The mean, standard deviation, and the variance were calculated over all three months at 0000 UTC and 1200 UTC to quantify the diurnal variability. In addition, the data were categorized by the model analyzed geostrophic wind direction and by the observed wind speed. The mean, standard deviation, and variance were then calculated for each separate category over the three months at 0000 UTC and 1200 UTC. The categories for the observed wind speeds were from 0-5 m/s, 5-10 m/s, and 10-17 m/s with 17 m/s the upper bound of the data set, and the geostrophic wind direction was classified as either onshore or offshore directed.

IV. RESULTS

The coastal winds are sensitive to the synoptic-scale flow characteristics in several ways. First, the synoptic-scale pressure gradient in part determines the strength of the coastal winds, which is consistent with the primary role that coastal baroclinity played in the coastal jet modeled by Burk and Thompson (1995). This can be seen by subjectively examining the synoptic surface charts, such as the example shown in Fig. 3. The highest winds at the coastal buoys tend to correspond to regions where the pressure gradient is somewhat larger. This basic dynamic result is further illustrated by a scatter plot of model-analyzed geostrophic wind speed versus observed wind speed shown in Fig. 4. The plot shows the weak tendency for the coastal winds at buoy 28 to be higher for the larger pressure gradients (geostrophic speeds). However, as seen in Fig. 4, there is considerable scatter, due to a variety of factors including analysis error and scale differences between observed winds and synoptic-scale analyses. One example of these differences is shown in Fig. 5, where the 20 kt observed wind at buoy 28 occurred under a relatively weak pressure gradient. In other cases, the synoptic-scale pressure gradient is relatively strong while the buoy 28 winds are rather weak. This shows that the

synoptic-scale pressure gradient is only partly reflective of the forcing of the coastal winds.

Second, the orientation of the synoptic-scale pressure gradient was found to play a significant role in shaping the coastal winds at buoy 28. The mean observed wind at buoy 28 for the three month period (75 days of usable data) for both 0000 UTC (Table 1) and 1200 UTC (Table 2) is approximately a factor of two larger when the model-analyzed geostrophic wind direction is offshore compared to onshore. The statistics in Tables 1 and 2 were computed using 76 and 75 data points respectively. The angle of the coastline near Point Sur was determined to be 345° true. The offshore model-analyzed geostrophic flow directions for the three month period ranged from 346° true through 360° to 093° true with most of the events occurring between 350° and 050° true. The onshore model analyzed geostrophic flow directions for three month period ranged from 196° to 345° true with most of the events occurring between 325° and 344 ° true. The range of model-analyzed geostrophic wind directions is rather small and represents the tendency of the synoptic analysis to position the low pressure along the coast of California. If the thermal low extends north of San Francisco and is displaced westward in the analyses, onshore geostrophic flow occurs near buoy 28. If the thermal low is well to the south or further inland,

offshore geostrophic flow is observed. Offshore and onshore represent the synoptic-scale analysis placement of features which may not be consistent with a more detailed analysis. However, offshore cases typically occur with a developing thermal trough while onshore cases represent mature thermal troughs.

To illustrate the observed wind speed variability for model-analyzed onshore and offshore geostrophic wind directions, scatter plots of the buoy 28 observed wind speeds versus the model-analyzed geostrophic wind direction were made. The distribution of winds for offshore geostrophic flow directions (Fig. 6) illustrates the tendency for higher wind speeds (7-14 m/s) to occur with these offshore flow directions, although lower speed events do occur. In contrast, the distribution of observed wind speeds for model analyzed geostrophic onshore flow directions (Fig. 7) show a tendency to cluster at lower observed wind speeds (below 6 m/s), although the sample size is substantially smaller.

These differences in mean observed wind speeds for offshore and onshore model-analyzed geostrophic flow directions may be a reflection of the tendency for weaker geostrophic winds (pressure gradient) to occur for the onshore flow direction. The mean geostrophic wind speed for onshore versus offshore was found to be lower, however for similar

model-analyzed geostrophic wind speeds with onshore and offshore orientation a systematic difference in the buoy 28 observed winds does occur. This is illustrated in Fig. 8 and Fig. 9, which are the synoptic surface analyses for 15 July 0000 UTC and 15 August 1200 UTC, respectively. The pressure analysis for 15 July in Fig. 8 indicates a relatively strong pressure gradient offshore which weakens substantially at the coast. In contrast, the pressure gradient for 15 August in Fig. 9 is relatively strong both offshore and inland of the coast, although its orientation changes dramatically. The geostrophic wind difference charts for the two cases (Fig. 10 & Fig. 11) show rather similar model-analyzed geostrophic speeds, approximately 10 and 12 m/s respectively. The observed buoy 28 winds for 15 July and 15 August differ markly at 10 and 20 kt, (Fig. 8 and Fig. 9), which supports the idea that the pressure gradient orientation (onshore/offshore) plays a role in determining the coastal winds beyond that due to the pressure gradient magnitude alone.

The diurnal variability of the coastal winds was examined statistically and from a synoptic perspective. The buoy 28 statistics suggest that the surface reflection of the California Coastal Jet does not exhibit any significant diurnal variation in the mean. This is illustrated in Table 1 and Table 2, which show the mean value of the observed winds

16

for the three month period for 0000 UTC is 8.05 m/s and for 1200 UTC is 8.67 m/s. The difference is about half a meter per second lower at the 0000 UTC evening time than the 1200 UTC morning, which is opposite to the expected diurnal tendency. The day to day variability , as reflected by the standard deviations of 3.5 and 4.0 m/s, is much more pronounced than the mean diurnal variability. The synoptic model shows a tendency to over-relax the pressure and thermal gradients on the 1200 UTC analysis. The diurnal variation in the model-analyzed winds is evident in Fig. 12 and Fig. 9, which show the model surface analysis charts with the observed winds for 0000 UTC and 1200 UTC on the 15th of August. The observed winds at buoy 28 are 20 knots on both the 0000 UTC and 1200 UTC charts. However, the model analyses show that the thermal and pressure gradients undergo some relaxation at 1200 UTC compared to 0000 UTC as the solar heating is absent during the night. As the statistics imply, August 15th is not an isolated case. Rather, it is a typical 24 hour period during the summer regime that demonstrates the persistence of the surface reflection of the coastal jet through the evening, contrary to the basic forcing by the coastal baroclinity.

To better understand the relationship between ETA model synoptic analyses and the coastal jet, the wind deviation (analysis error) at buoy 28 was examined. As evident in

17

Tables 1 and 2, and as mentioned above, the model analyzed winds are substantially below those actually observed at buoy 28. The deviation is almost 5 m/s at 0000 UTC when the synoptic-scale pressure gradient is stronger and jumps to 6.5 m/s at 1200 UTC when the large-scale pressure gradient relaxes. This suggests that the model-analyzed pressure gradient is systematically too low and that its diurnal variation may be overestimated. Evidently the pressure analysis at 0000 UTC during the warm part of the diurnal cycle is more reflective of the "local" pressure gradient affecting buoy 28 winds. The rather large 5 m/s deviation at 0000 UTC indicates that mesoscale coastal effects are significant in explaining the rather strong surface winds at buoy 28.

To assess the possible impact of flow blocking and supercritical flow effects on the buoy 28 winds, the deviation of the observed wind from the model-analyzed wind was broken down into three wind speed categories. For the 1200 UTC time, the wind deviations from the model were 4.6, 6.2, and 8.1 m/s for the 0-5, 5-10, and 10-17 m/s categories as seen in Table 2. This suggests that the model underestimate of the coastal winds is simply proportional to the overall pressure gradient. Larger (smaller) deviations occur for larger (smaller) pressure gradients. For the 0000 UTC time, when the model winds are generally more realistic, the wind deviations were

3.3, 4.4, and 7.2 m/s for the 0-5, 5-10, and 10-17 m/s categories as seen in Table 1. Interestingly, the deviation of the observed winds increases sharply for the higher wind speeds. This suggests that for the higher wind speeds mesoscale effects may play a more significant role in determining the actual wind.

To better illustrate the wind speed dependence, scatter plots of the observed winds versus the model winds were produced (Figs. 13 and 14) for 0000 UTC and 1200 UTC, respectively. Figure 13 illustrates that a simple linear regression doesn't fit the data well. Rather, a non-linear relationship exist between the model error and the observed wind. However, using approximately 8.5 m/s as a cut off between higher and lower wind speeds, the data seems to exhibit somewhat linear behavior. While the model is reasonably handling the magnitude of the wind (i.e., the thermal and pressure gradients support the observed wind to some degree) for lower wind speeds, the slope of the best fit line increases significantly for higher wind speeds. The deviation for the higher observed wind speeds is greater and increasing more rapidly than for the lower observed wind speeds. This suggests that the model is still unable to resolve effects that are causing the higher observed wind events. In contrast, the slope of the best fit line in Fig.

14, for the 1200 UTC data, is more linear and not as steep. However, the mean error on the 1200 UTC chart is greater. This suggests that the error on the 1200 UTC chart is more a result of the ETA model over-relaxing the thermal and pressure gradients and less a result of the models inability to resolve the mesoscale effects. Together these suggest that the strength of the synoptic-scale thermal and pressure gradients is the dominant factor in getting the surface reflection of the coastal jet wind speeds correct. However, as the winds increase mesoscale effects begin to increase the observed winds beyond that suggested by the large-scale pressure gradient. Potentially, this is the result of supercritical flow which is more prevalent for higher wind speeds.

To try to understand the nature of the forcing for the high wind events better, the soundings and upper-level winds were examined for cases subjectively identified as having strong observed winds. Figure 15 shows the surface analysis as an example of one of these cases. In this example, 20 kt buoy 28 winds are observed under a moderately strong pressure gradient that yields a geostrophic wind of about 15 m/s (30 kt) at buoy 28. A sounding taken by the RV SPROUL (Fig. 16), offshore from Pt. Sur, shows 30 kt surface winds below a rather strong inversion at a height of 300 m. Above the marine layer, pronounced southerly and southwesterly flow are

evident, suggesting the approach of an upper-level trough. Through examination of similar plots for other cases of 20 kt or greater winds at buoy 28, the upper-level flow and the height of the inversion were found to be highly varied. Northwesterly flow aloft and deeper marine layers were also found to produce strong winds at buoy 28, which suggests that the winds in the marine boundary layer are largely unaffected by the flow above the marine boundary layer. Although the height and strength of the inversion varied considerably, it was generally below the height of the coastal mountains and sufficiently strong to produce flow blocking for cross-coast winds less than 5-10 m/s. Consequently, the potential for flow blocking and supercritical effects is high for these days. Qualitatively, the strength of the observed winds at buoy locations near Monterey and Big Sur showed little dependence on the height or strength of the inversion. However, a more detailed analysis of the relationship between the height and strength of the inversion and the coastal surface winds is needed.

V.   DISCUSSION AND CONCLUSIONS

This study has found three significant characteristics of the California Coastal Jet as reflected in the surface winds at buoy 46028 and its relationship to synoptic-scale structure. First, the California Coastal Jet, as observed at buoy 28, exhibits a strong dependence on synoptic-scale flow direction. When the model-analyzed geostrophic wind direction is offshore, the observed winds along the coast are on average a factor of two stronger than when the model-analyzed geostrophic wind is onshore. Although the along-shore pressure gradient tends to be less for periods of geostrophic onshore flow, higher coastal winds result under geostrophic offshore flow for comparable pressure gradients. For a given pressure gradient, the greater its along-shore component the greater the coastal winds are likely to be. Although not analyzed in this study, the author speculates that for geostrophic offshore flow, the flow in the marine boundary layer is blocked by the coastal topography and so tends to accelerate down the pressure gradient to yield a strong coastal jet. Conversely, when the geostrophic wind direction is onshore, the flow in the marine boundary layer tends to be in a more balanced, quasi-geostrophic state, where no additional energy is imparted to the coastal winds due to flow

23

blocking of a cross-coast wind component.

Second, the California Coastal Jet exhibits little or no diurnal variation. The mean value of the observed wind at buoy 28 for the 1200 UTC time during the three month period was one-half a meter per second greater than the mean value during the 0000 UTC time, which is far less than the day-to-day variability. Although the observed winds exhibit little diurnal variation, the synoptic-scale thermal and pressure gradients exhibit substantial diurnal·variation as seen in the model-analyzed winds, the deviation in the model-analyzed winds from the observed winds is substantially larger at 1200 UTC. Evidently, either the synoptic analyses greatly under-analyze the coastal baroclinity at 1200 UTC times or additional mesoscale factors contribute to maintaining the coastal winds at night.

Finally, for periods when the coastal winds are strong (pronounced jet) the synoptic-scale analyses provide the least accurate indication of the coastal winds. When the winds along the coast are light to moderate, the synoptic-scale thermal and pressure gradients adequately indicate the primary forcing of the coastal winds. This is particularly true at 0000 UTC when the model diurnal bias is minimized. However, when the winds are strong, the ability of the synoptic-scale analyses to represent the forcing of the coastal winds

24

decreases. This implies that either the analysis error is substantially larger for these times or that other mesoscale effects, such as supercritical flow effects, contribute more substantially to the observed winds at these times. Given the wind speed dependence, it is likely that supercritical flow acceleration is responsible for the enhancement of the winds above their synoptic-scale estimates.

VI. RECOMMENDATIONS

The study has demonstrated that the California Coastal Jet is sensitive to the synoptic-scale flow and that mesoscale effects may be responsible for the enhancement of the winds along the coast. Future studies should be conducted that look at the results and differences found in this study using other higher resolution model analyses such as MM5 or COAMPS. The higher resolution model would possibly capture more of the mesoscale effects and better separate the effects of the synoptic-scale forcing and analysis deficiencies.

It is also recommended that the stability and inversion characteristics be examined to help understand the role of the marine layer and the inversion in causing deviations from the synoptic-scale forcing. Calculation of the Froude number and classifying the observed and model-analyzed winds by the Froude number would be useful. A more complete data set obtained in 1996 could be used to extend the study.

Finally, a more thorough examination of the synoptic-scale structure above the marine boundary layer and its relationship to the surface synoptic condition is needed. The transition from geostrophic onshore to offshore flows is probably related to synoptic changes aloft. But this has not been examined. In general, the coastal winds are

27

northwesterly and the pressures are high offshore and low inland, however, this basic flow occurs under both northwesterly and southwesterly flow at 850 mb. The impact of the flow differences at 850 mb on the winds below the inversion is not known and should be examined.
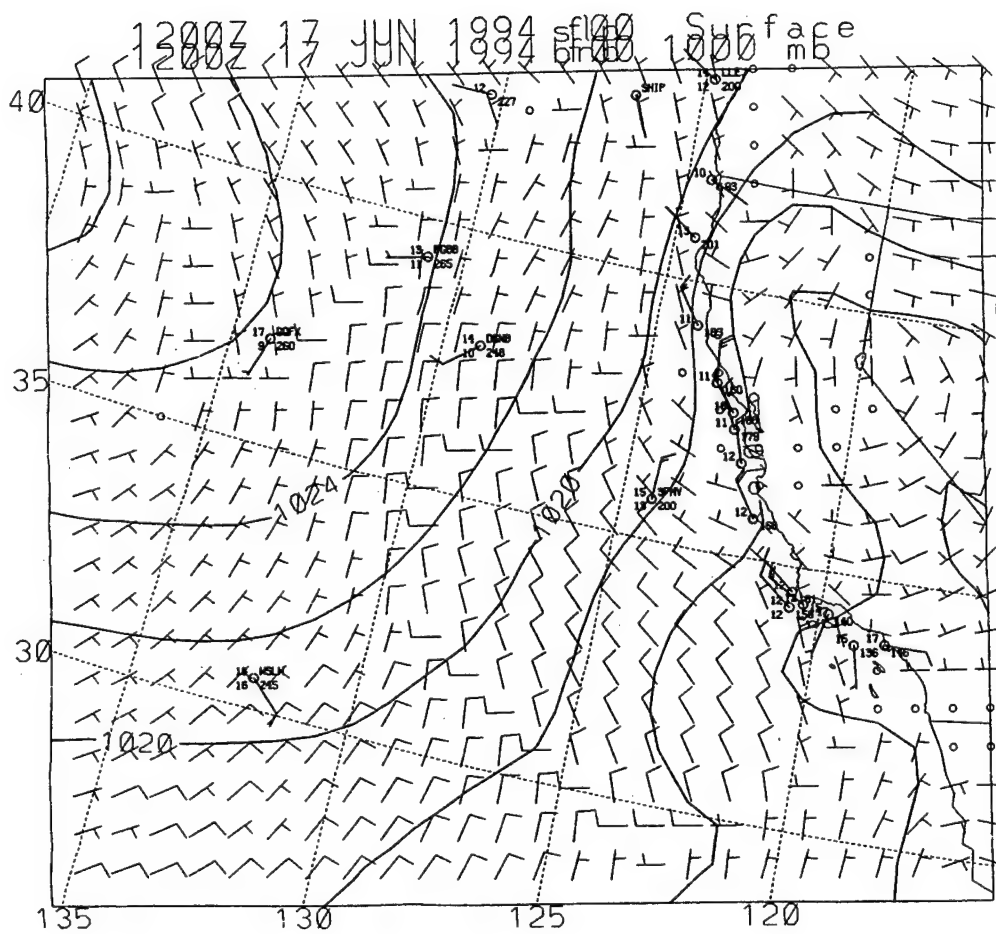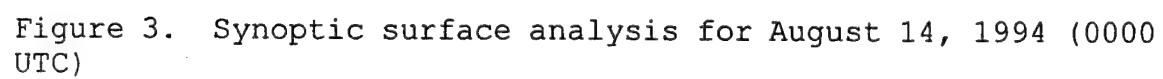
Figure 1. Example of a difference plot. The difference winds at the observation sites are the observed winds minus the modeled winds. Modeled winds are in m/s and the difference winds are in kt
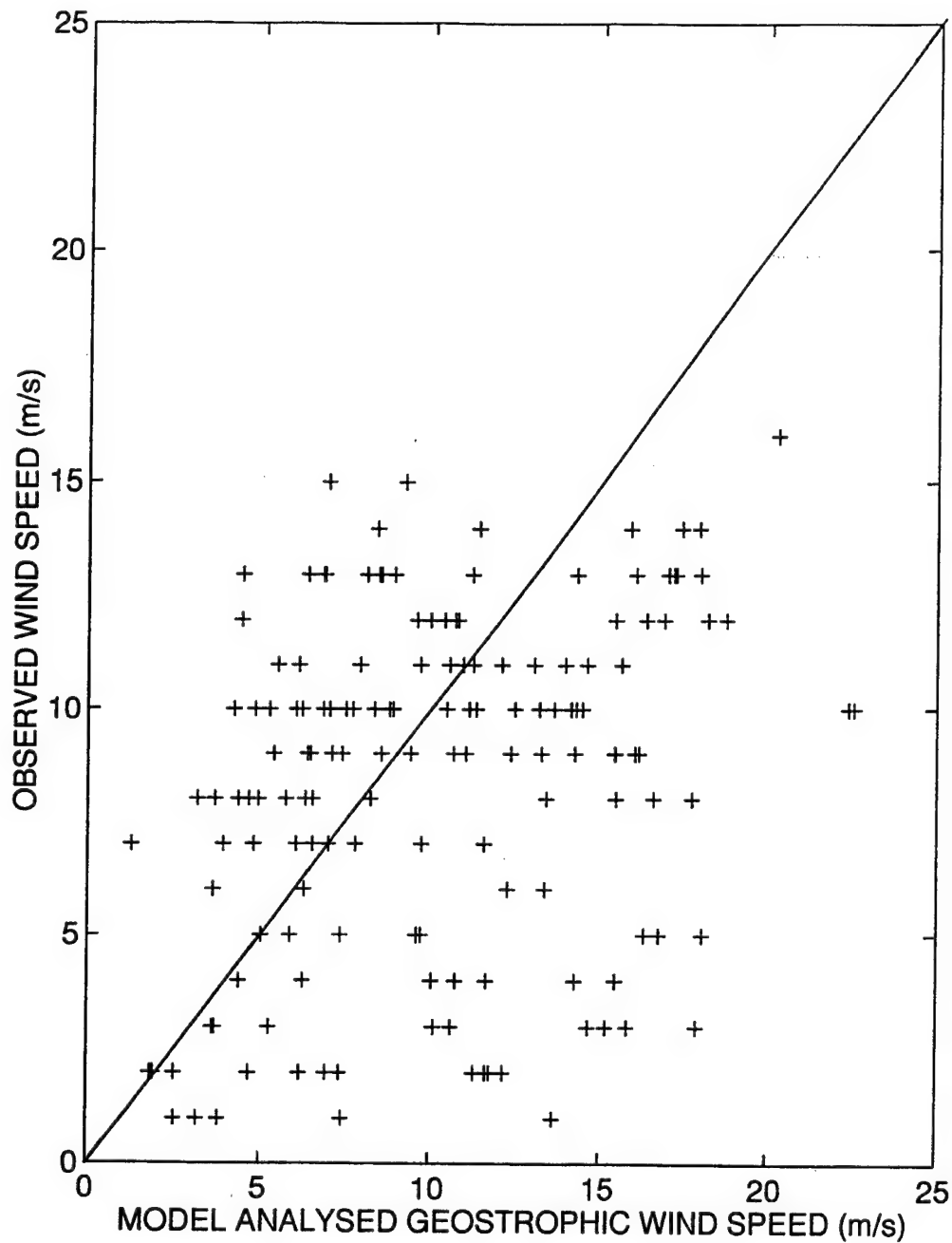
29

Figure 2. Example of a vector plot illustrating the geostrophic wind direction and the relative magnitude with differences (observations minus the modeled geostrophic) plotted at the observation sites

Figure 3.   Synoptic surface analysis for August 14, 1994 (0000 UTC)

Figure 4. Scatter plot of the model analyzed geostrophic wind speed versus the observed wind

32

Figure 5.   Synoptic surface analysis for July 01, 1994
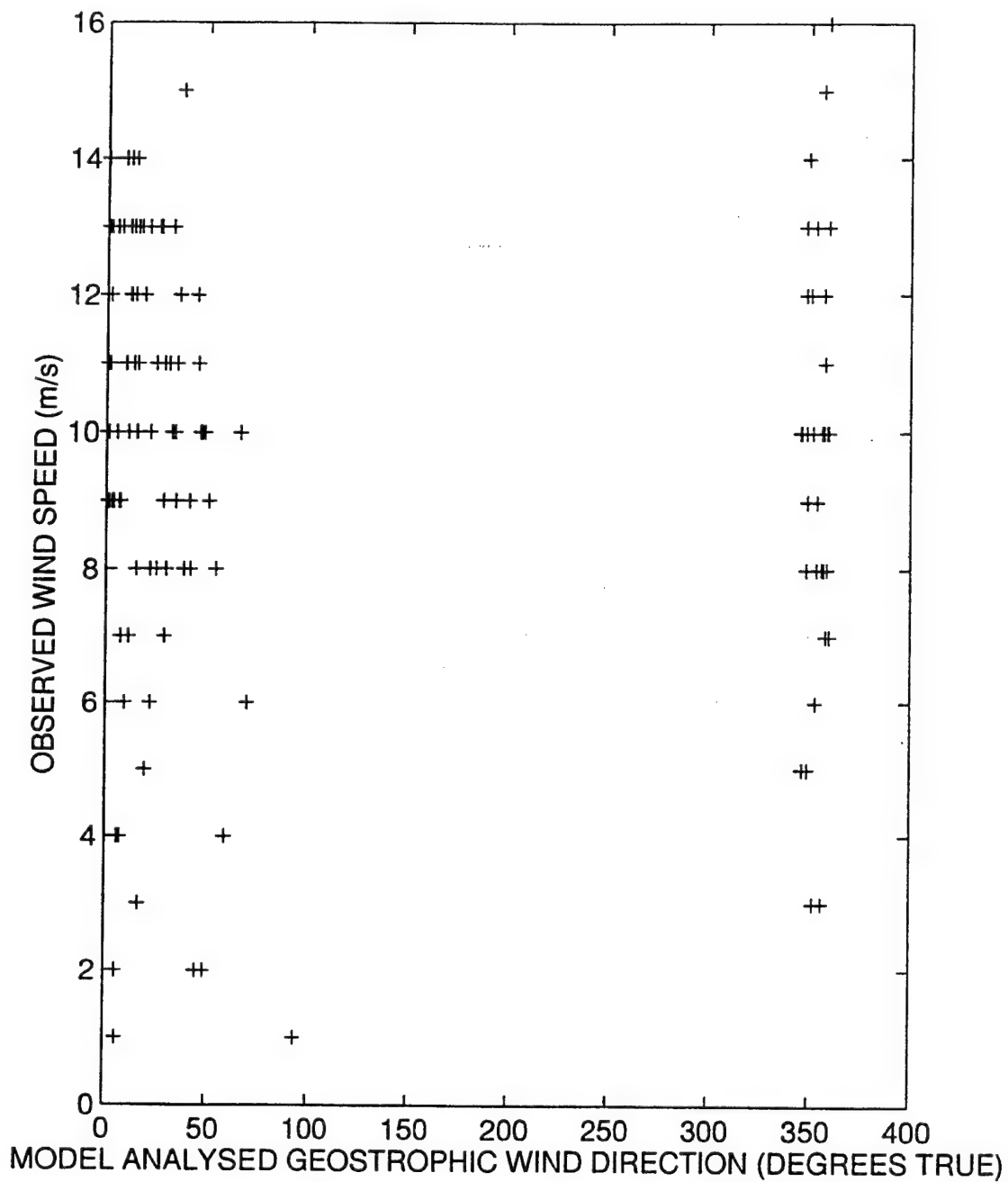
Figure 6.   Scatter plot of the buoy 28 observed wind speeds
versus the offshore model analyzed geostrophic wind direction
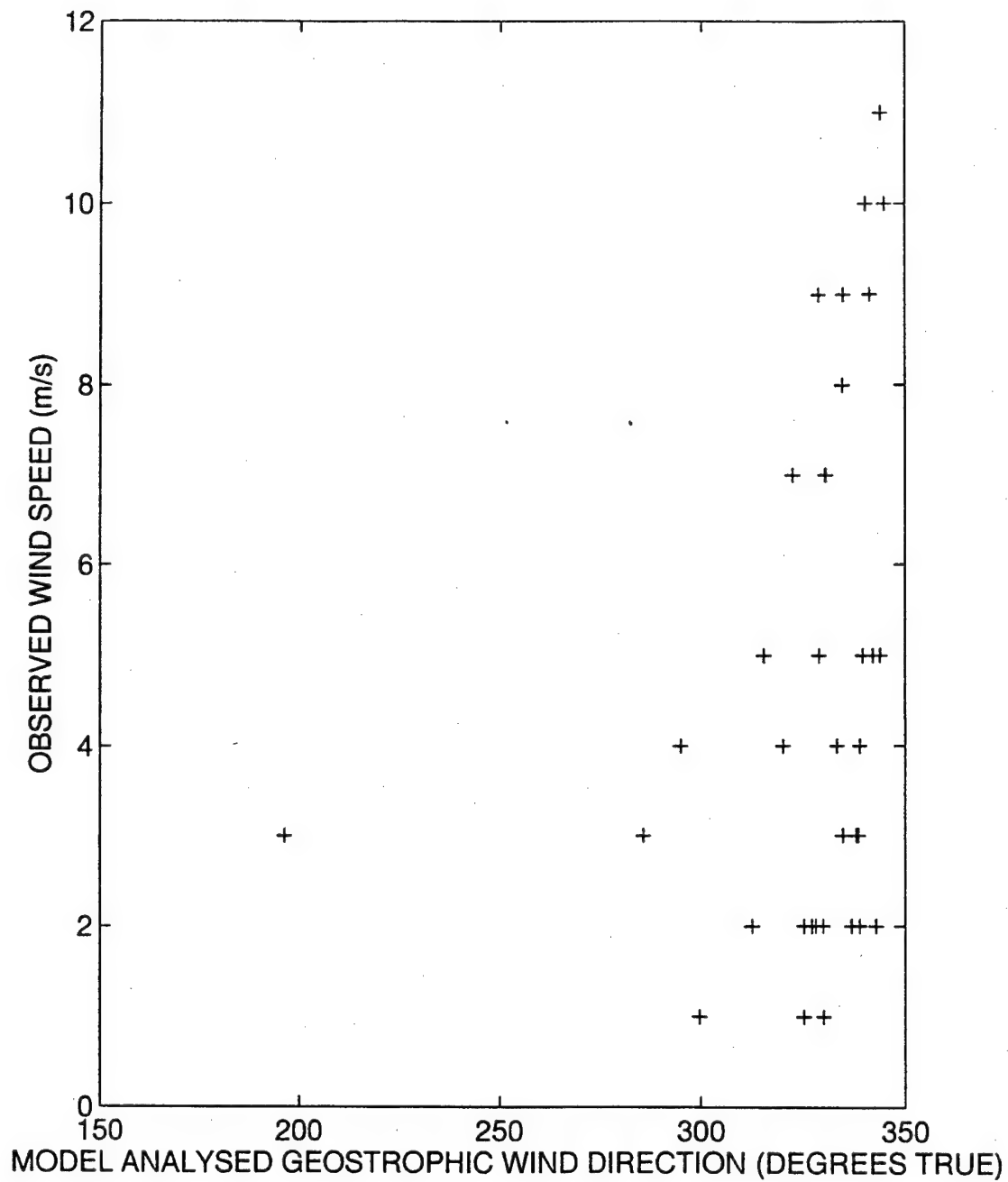
Figure 7. Scatter plot of the buoy 28 observed wind speeds versus the onshore model analyzed geostrophic wind direction
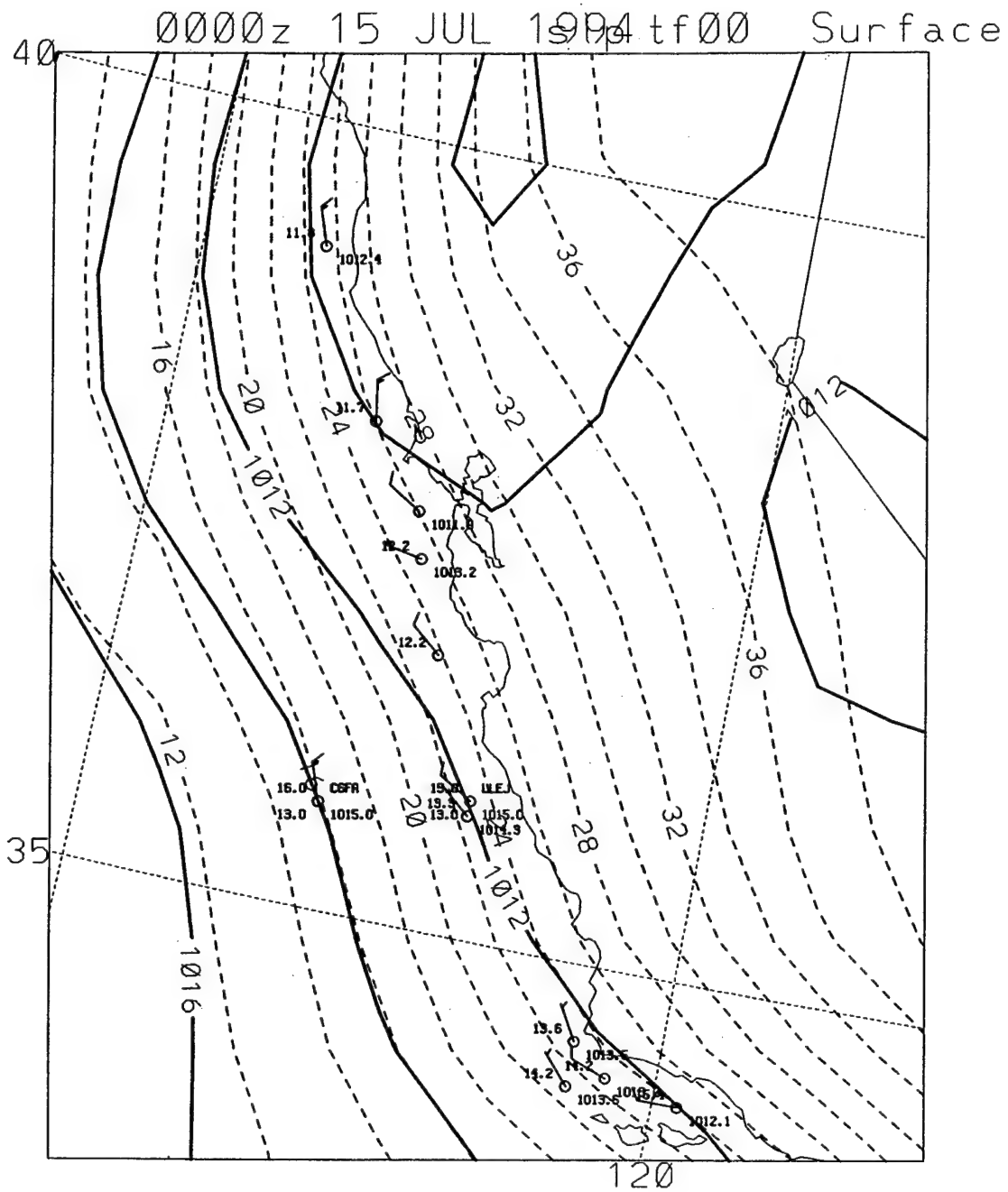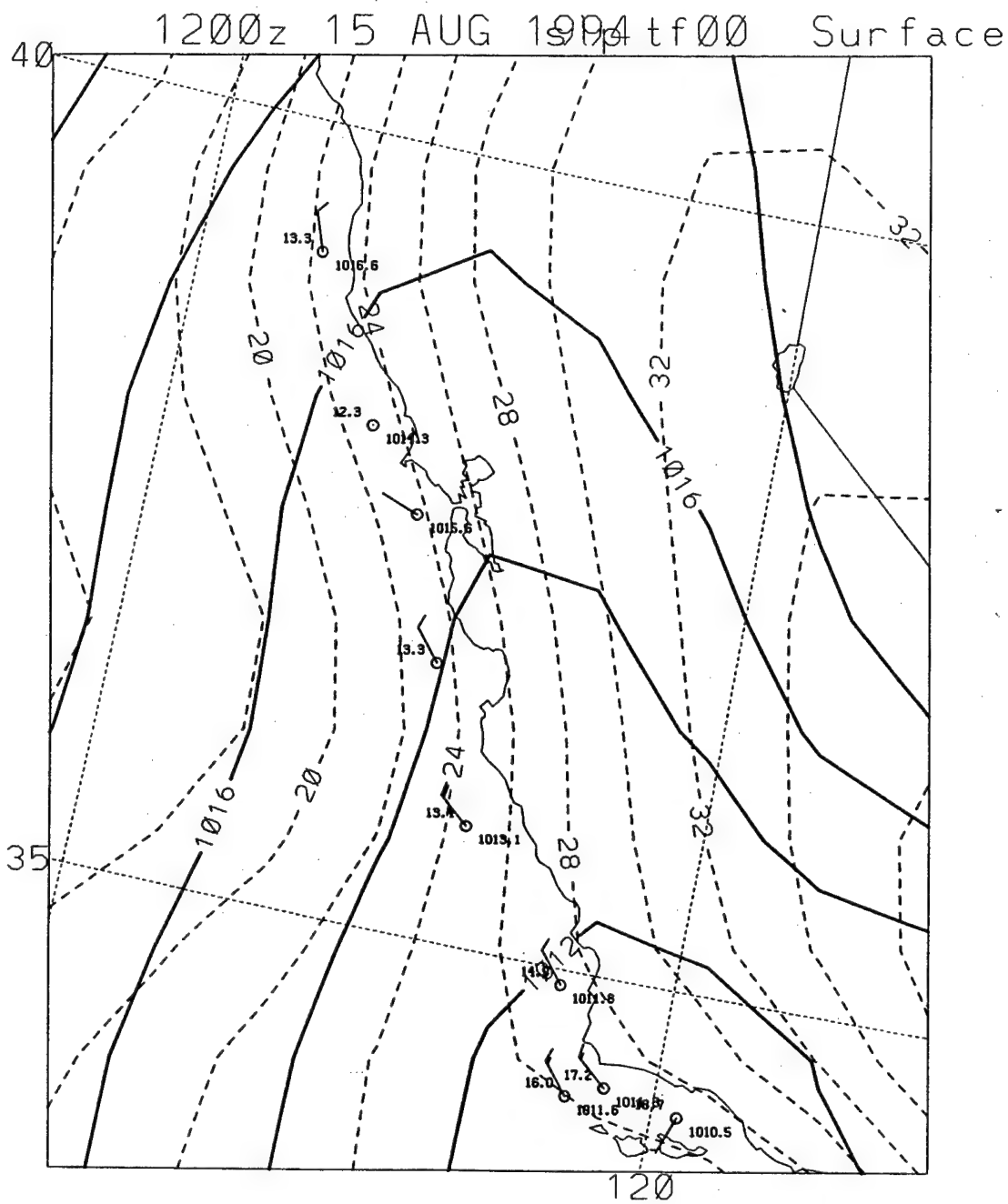
Figure 8. Synoptic surface chart for July 15, 1994 (0000 UTC)

Figure 9.   Surface synoptic chart for August 15, 1994 (1200 UTC)
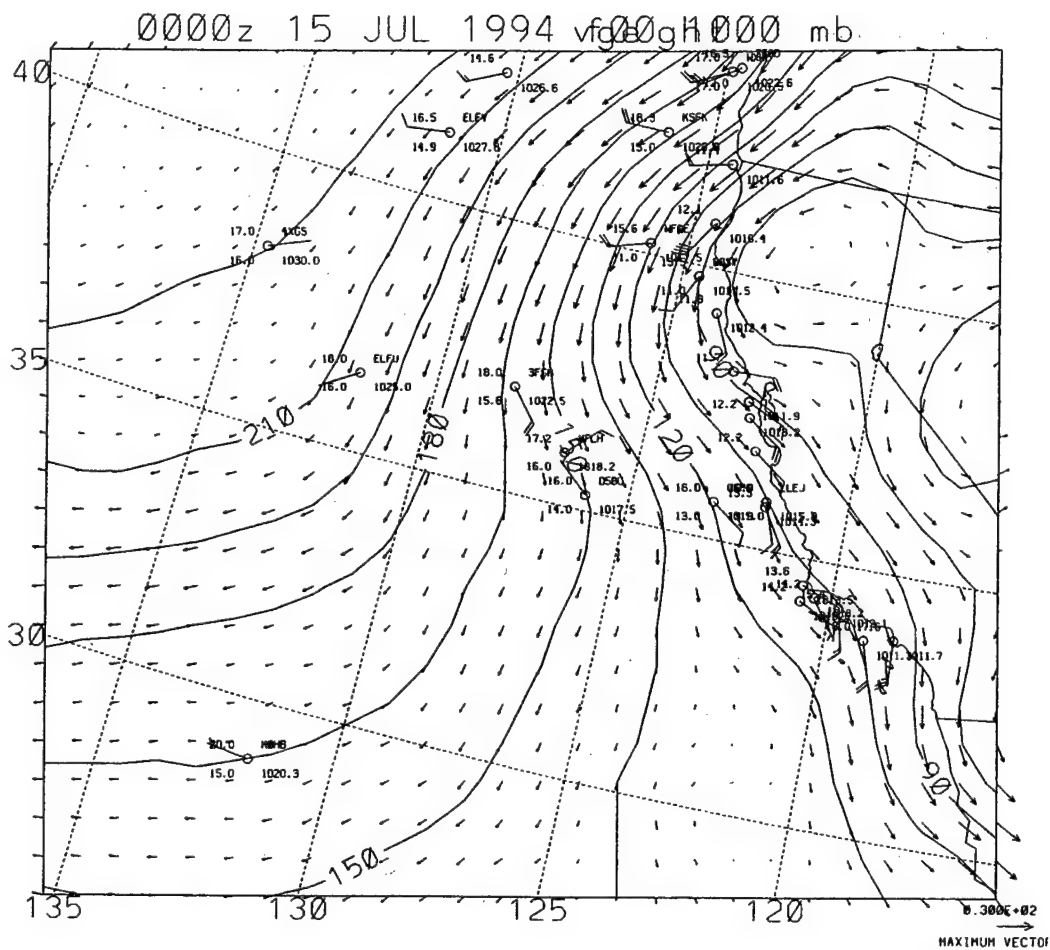
37

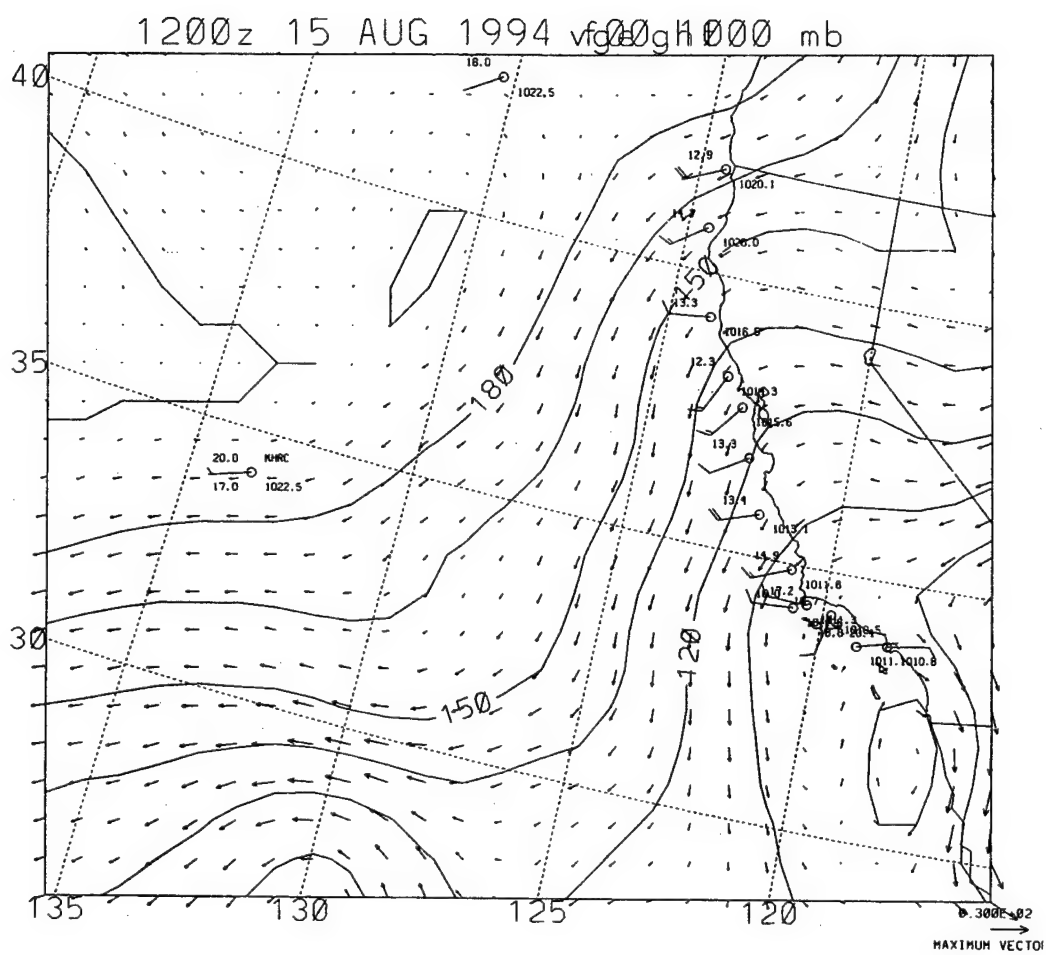Figure 10.   Vector plot of the geostrophic wind for July 15, 1994 (0000 UTC)

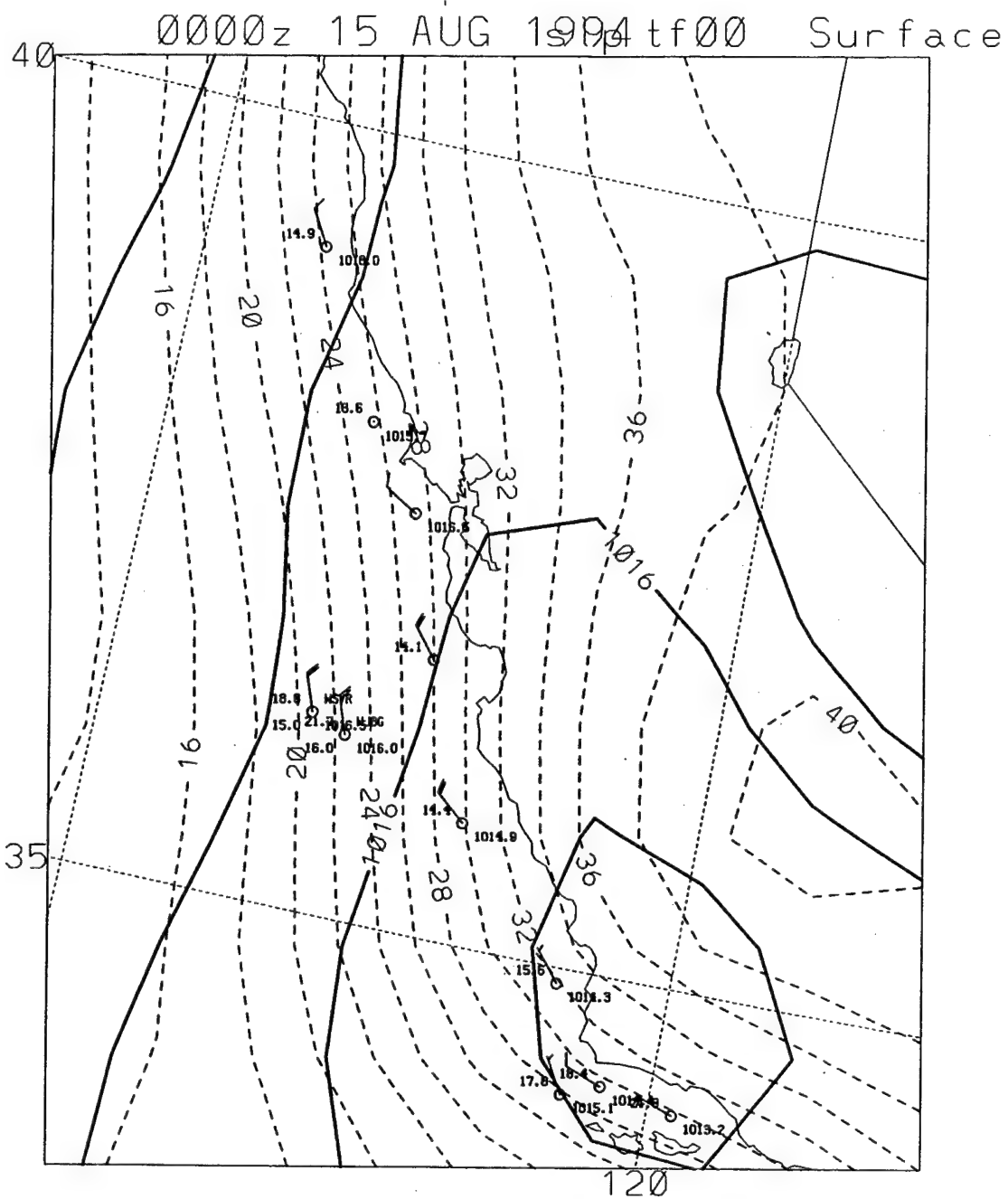Figure 11.   Vector plot of the geostrophic wind for August 15, 1994 (0000 UTC)

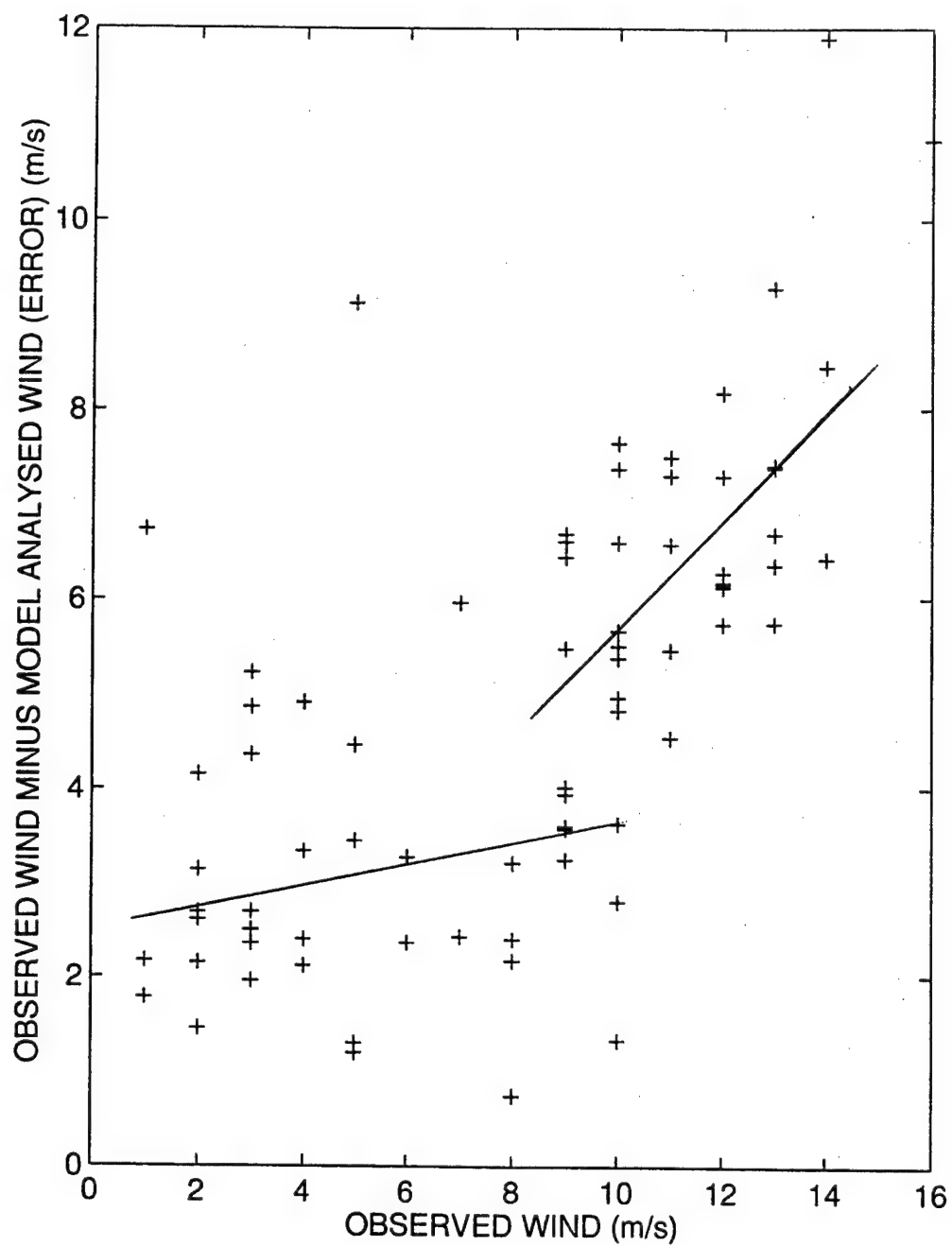Figure 12.   Synoptic surface chart for August 15, 1994 (0000 UTC)

40

Figure 13. Scatter plot of the buoy 28 observed wind speeds versus the model analyzed winds for 0000 UTC
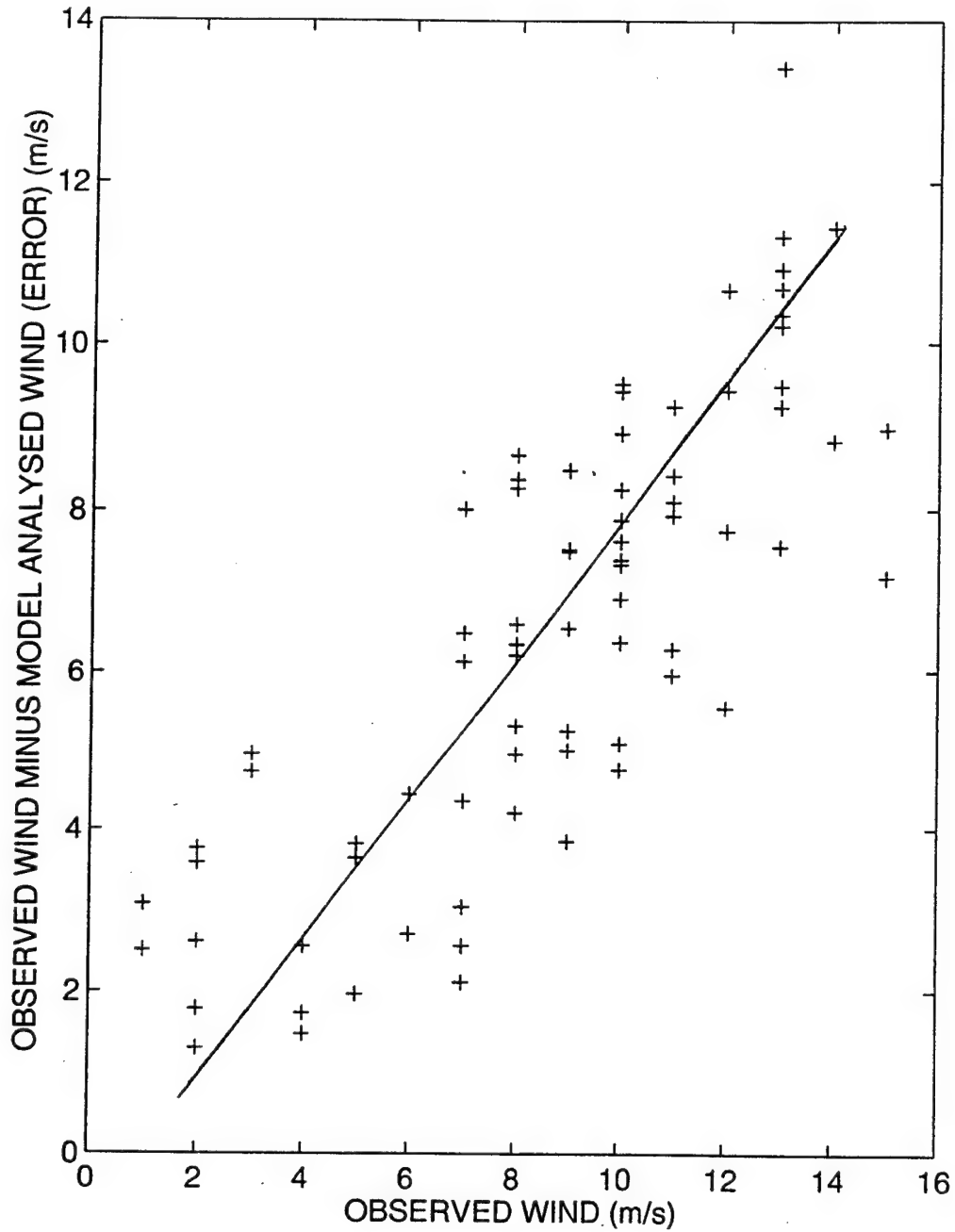
Figure 14. Scatter plot of the buoy 28 observed wind speeds versus the model analyzed winds for 1200 UTC
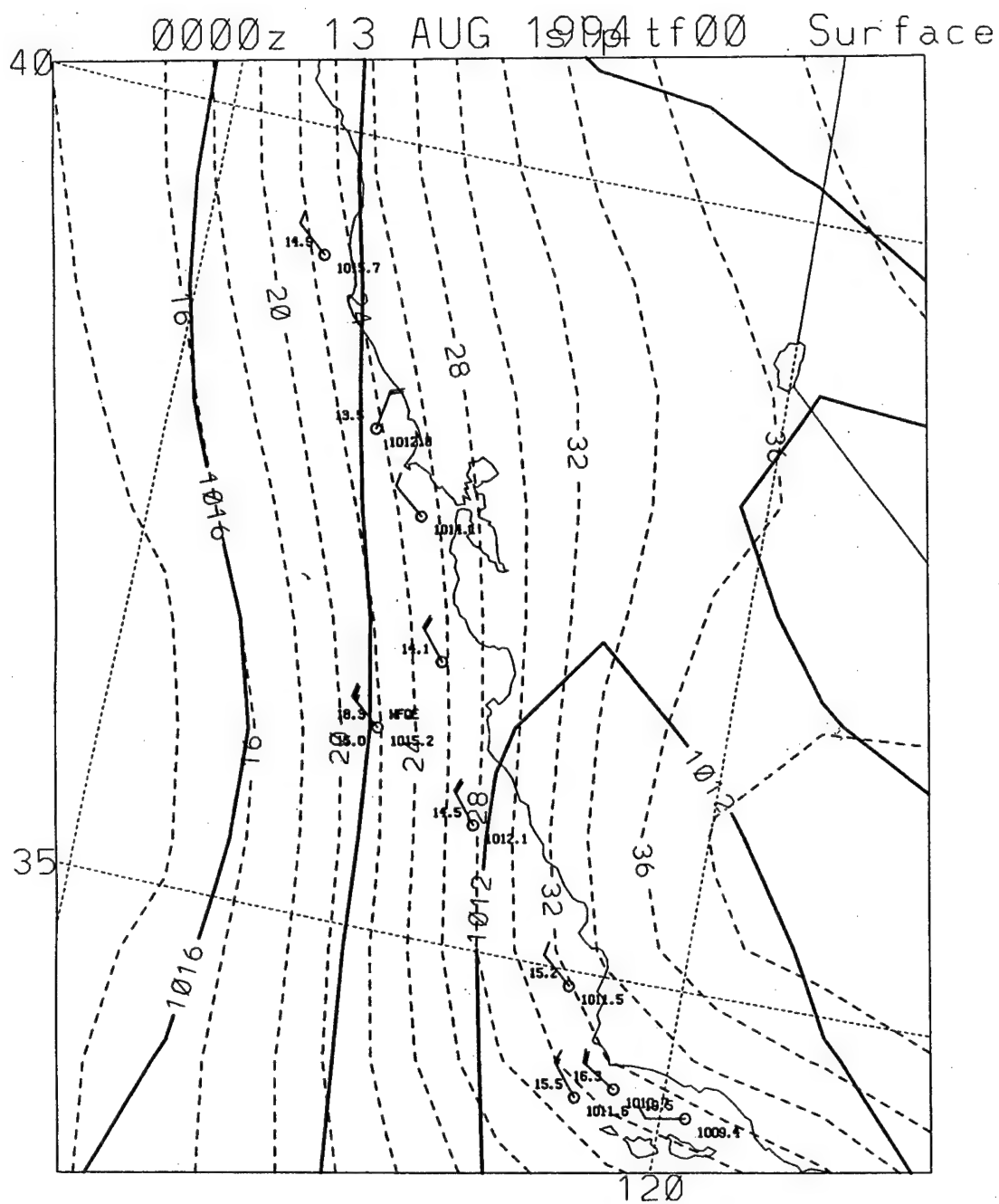
Figure 15. Synoptic surface analysis for August 13, 1994 (0000 UTC)

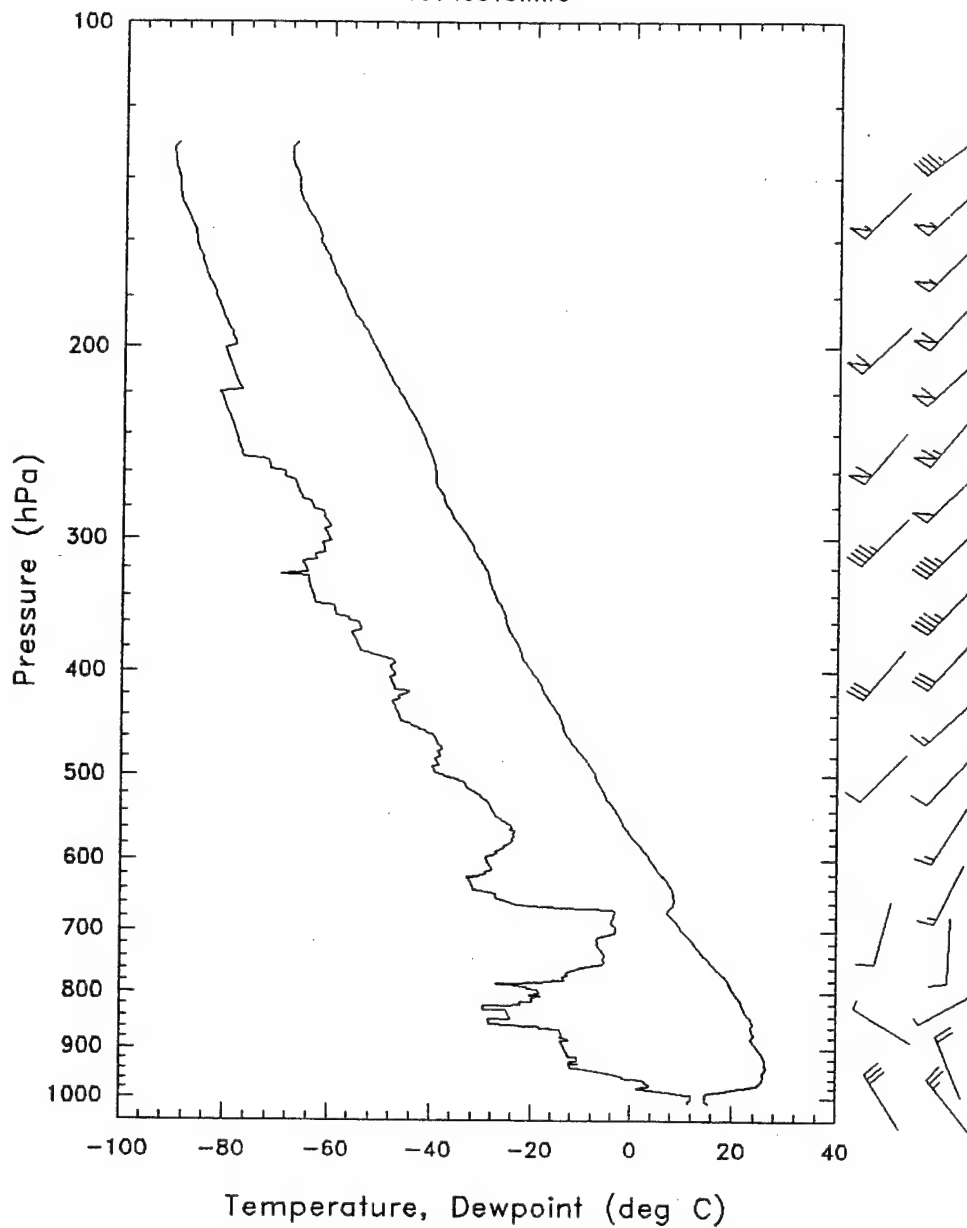R/V Sproul 36.41 N 122.23 W   13 AUG 94   1:00 GMT

r0940813.mrs

Figure 16.   Sounding taken by RV SPROUL offshore from Point Sur on August 13, 1994, at 0100 UTC

PARAMETER	MEAN	STANDARD DEVIATION
OBSERVED WIND	8.0526	3.9963
MODEL ANALYZED WIND	5.4940	1.5933
ERROR WIND	4.8722	2.3924
MODEL GEOSTROPHIC WIND	13.7938	3.6138
OBSERVED WIND FOR GEOSTROPHIC OFFSHORE	9.6731	3.2643
OBSERVED WIND FOR GEOSTROPHIC ONSHORE	4.5417	3.1065
OBSERVED WIND (0-5)	3.000	1.2854
OBSERVED WIND (5-10)	8.7586	1.4055
OBSERVED WIND (10-17)	12.4348	1.2730
MODEL ANALYZED WIND FOR OBS(0-5)	4.8721	1.4978
MODEL ANALYZED WIND FOR OBS(5-10)	5.7572	1.8792
MODEL ANALYZED WIND FOR OBS(10-17)	5.8111	1.0935
ERROR FOR OBS(0-5)	3.2780	1.8636
ERROR FOR OBS (5-10)	4.3593	1.8450
ERROR FOR OBS(10-17)	7.1824	1.6884

Table 1. Results of the statistical analyses performed on the buoy 28 data for 0000 UTC. All speeds in m/s

PARAMETER	MEAN	STANDARD DEVIATION
OBSERVED WIND	8.6667	3.5880
MODEL ANALYZED WIND	3.5286	1.8328
ERROR WIND	6.4691	2.8361
MODEL GEOSTROPHIC WIND	6.5504	2.4269
OBSERVED WIND FOR GEOSTROPHIC OFFSHORE	9.4677	3.2478
OBSERVED WIND FOR GEOSTROPHIC ONSHORE	4.8462	2.5770
OBSERVED WIND (0-5)	3.0000	1.4142
OBSERVED WIND (5-10)	8.4118	1.2581
OBSERVED WIND (10-17)	12.2692	1.4299
MODEL ANALYZED WIND FOR OBSERVED (0-5)	2.8391	1.1245
MODEL ANALYZED WIND FOR OBSERVED(5-10)	3.3163	1.9007
MODEL ANALYZED WIND FOR OBS(10-17)	4.2040	1.9094
ERROR FOR OBS (0-5)	4.6484	1.1522
ERROR FOR OBS(5-10)	6.1933	2.0627
ERROR FOR OBS(10-17)	8.1146	2.0093

Table 2. Results of the statistical analyses performed on the
buoy 28 data for 1200 UTC. All speeds in m/s

46

LIST OF REFERENCES

Black, T.,Deaven, D. DiMego, G., 1993: National Weather Service Technical Procedures Bulletin, Series No. 412, available from the National Centers for Environmental Prediction, Washington, D.C.

Burk, S. D. And Thompson, W. T., 1995: The summertime low-level jet and marine boundary layer structure along the California coast. *Mon. Wea. Rev.,***124**, 668-686.

Nuss, W. A. And Drake, S., 1993: Visual, Meteorological Diagnostic and Display Program User's Guide. Available from the Naval Postgraduate School, Department of Meteorology.

Winant, C. D., Dorman, C. E., Friehe, C. A., Beardsley, R. C., 1988: The marine layer off Northern California: An example of supercritical flow., *J. Met. Sci.,***45**,3588-3605.

INITIAL DISTRIBUTION LIST

No. Copies

1.   Defense Technical Information Center   2
8725 John J. Kingman Rd., STE 0944
Ft. Belvoir, VA 22060-6218

2.   Dudley Knox Library   2
Naval Postgraduate School
411 Dyer Rd.
Monterey, CA 93943-5101

3. Chairman, Code MR   1
Department of Meteorology
Naval Postgraduate School
Monterey, CA 93943-5002

4. Professor Wendell A. Nuss   1
Department of Meteorology
Naval Postgraduate School
Monterey, CA 93943-5002

5. Professor Patricia M. Pauley   1
Department of Meteorology
Naval Postgraduate School
Monterey, CA 93943-5002

6. Commanding Officer   1
Fleet Numerical Meteorology and Oceanography Center
7 Grace Hopper Ave
Monterey, CA 93943-5501

7. LCDR Eugene P. Tramm   1
PSC 1003, Box 26
FPO AE 09728-0326

8. LT R. Scott Stevens   2
3340 Del Monte BLVD APT 20
Marina CA 93933